ELSEVIER

Journal of Nuclear Materials 278 (2000) 334–345

journal of nuclear materials

www.elsevier.nl/locate/jnucmat

Long-term corrosion of Zircaloy before and after irradiation

E. Hillner, D.G. Franklin *, J.D. Smee

Bechtel Bettis Inc., Bettis Atomic Power Laboratory, P.O. Box 79, West Mifflin, PA 15122, USA

Received 5 May 1998; accepted 12 August 1999

Abstract

Recently analyzed long-term Zircaloy autoclave corrosion data were used to develop new Zircaloy corrosion correlations. Twenty-two different autoclave tests were analyzed. The tests included specimens from 46 different heats, of both Zircaloy-2 and Zircaloy-4. The material conditions included different heat treatments and various prefilms. Approximately 14 500 data points were generated. Maximum exposure time was 10 507 days (~29 yr) in a 316°C, test and maximum weight gain was 1665 mg/dm^2 (~114 μm of oxide film) for a 338°C experiment. A single linear post-transition rate constant was determined in tests where maximum corrosion film thicknesses did not exceed ~30 μm. At the highest temperatures, where oxide film thicknesses in excess of ~30 μm were generated, the post-transition corrosion data can best be described by two successive linear equations, each active over a different range. Special in-reactor tests demonstrated that accelerated in-reactor effects on corrosion dissipate after growth of an additional oxide film, on the order of the thickness of the pre-transition oxide layer.

1. Introduction

Low-temperature ex-reactor (autoclave) corrosion of Zircaloy has undergone renewed interest recently due to considerations associated with the long-term storage of spent fuel elements from nuclear reactors. To date, the fuel-element cladding of choice for most nuclear power plants has been one of two Zircaloys, which are alloys of zirconium with small amounts of tin, iron, chromium, and nickel as alloying additions. Zircaloy-4 is used as cladding in pressurized water reactors (PWR) and in channels in some boiling water reactors (BWR). Zircaloy-2 is the common cladding used in BWRs. The two properties of zirconium alloys that largely influenced their selection for cladding are their excellent high-temperature water-corrosion resistance and very low thermal neutron absorption cross-section. Since these two Zircaloys exhibit similar corrosion behavior out of reactor, only the generic term 'Zircaloy' will be employed in this report. However, all discussions and conclusions in this document apply to both Zircaloy-2 and Zircaloy-4.

Under present considerations it is anticipated that the vast majority of repository exposure for the Zircaloy-clad spent fuel elements would take place at temperatures in the neighborhood of ~95°C and below. However, most Zircaloy autoclave data have been generated in the temperature range of 250–360°C in degassed deionized water and with relatively short exposure times for the lower test temperatures. The excellent corrosion resistance of Zircaloy makes it impractical to conduct meaningful isothermal autoclave testing below ~230°C in any reasonable time period, except in extreme water chemistries. Thus, it will be necessary to employ corrosion correlations based on data generated at the temperatures above 230°C and make extrapolations to the lower temperatures anticipated in the repositories.

Two primary tasks must be completed to provide a corrosion predictive tool for long-term storage of Zircaloy core materials. First, a corrosion database must be obtained and used to develop a correlation to predict corrosion. This report presents the results of 30 yr of out-of-reactor autoclave testing. This database provides corrosion rates for the lowest temperatures for which meaningful results could be obtained for the time period since the Zircaloys were developed. These data are used to develop a predictive correlation for Zircaloy

* Corresponding author. Tel.: +1-412 476 6573; fax.: +1-412 476 5151.

0022-3115/00/$ - see front matter
PII: S0022-3115(99)00230-5

corrosion. Second, the correlation must be shown to apply to Zircaloys after irradiation. The results of special in-reactor tests are used to support an assumption that in-reactor effects on the corrosion rate cease after a period of additional oxide growth. Two important literature results that support this assumption also are discussed.

2. Background

Zircaloy reacts with water to form a corrosion film of ZrO_2, by the following reaction:

$$Zr + 2H_2O \rightarrow ZrO_2 + 2H_2. \quad (1)$$

Since virtually all of the oxygen generated in Eq. (1) reacts with the Zircaloy to form the corrosion film and the film remains adherent, the weight gain of the corrosion specimens has been used as a direct gauge of the oxide film thickness. [1] The Zircaloy corrosion processes are known to occur in three stages:

1. The early pre-transition regime, characterized by the formation of a thin, black, tightly adherent corrosion film that grows thicker in accordance with a cubic rate law.
2. The midlife transition, or transitory stage, that lies between the pre-transition and post-transition stages. As initially shown by Bryner [1], this region appears to be comprised of series of successive cubic curves, similar to the initial cubic kinetic curve, but initiating at shorter and shorter intervals.
3. The linear post-transition kinetic regime.

The three-stage Zircaloy corrosion behavior is shown schematically in Fig. 1. The dashed lines in Fig. 1 indicate that most early corrosion models recognized only the pre-transition and post-transition kinetic regimes. Since some spent fuel cladding will be in the post-transition region upon entry into a repository, i.e., oxide film thicknesses in excess of 25 μm, this document will be concerned only with post-transition corrosion behavior. The use of these kinetics will be conservative for cladding that may not have attained the post-transition region prior to disposal. Post-transition corrosion kinetics can be described by an expression of the form

$$\Delta W = K_L t + C, \quad (2)$$

where ΔW is the specimen weight gain, in units of mg/dm^2, t the exposure time, in units of days, K_L the empirical constant, usually termed the linear (or post-transition) rate constant, in units of mg/dm^2/day, and C another constant, in the same units as ΔW (mg/dm^2), which is the intercept of the linear equation at zero time.

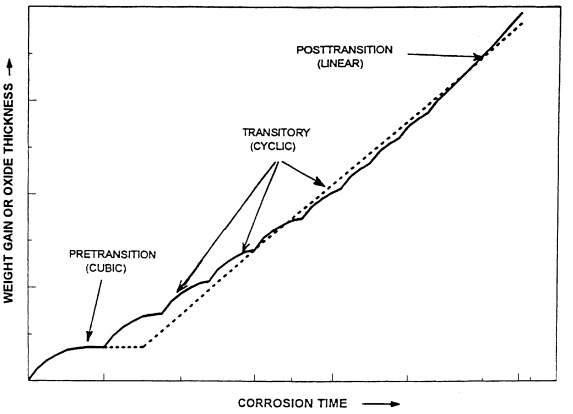

Fig. 1. Schematic drawing showing the three Zircaloy corrosion regions: pre-transition, transitory, and post-transition. The dashed lines indicate that early models recognized only the pre-transition and post-transition regimes.

From Eq. (2), a plot of the weight gain as a function of the exposure time produces a straight line with a slope equal to K_L and an intercept equal to the constant, C. The temperature dependence of the linear rate constant (K_L) has been shown to follow an Arrhenius-type behavior of the form

$$K_L = B \exp[-Q_L/RT], \quad (3)$$

where B is an empirical constant, in units of mg/dm^2/day, Q_L the activation energy for the post-transition (linear) corrosion region, in units of J/mol, R the universal gas constant, 8.31 J/mol K, and T the absolute temperature, in units of K.

Thus, from Eq. (3), a plot of the natural logarithm of the linear rate constant $[\ln(K_L)]$ against the reciprocal of the absolute temperature generates a straight line with a slope equal to $-Q_L/R$ and an intercept on the Y-axis equal to the natural logarithm of the constant, B. Combining Eqs. (2) and (3) results in the following general expression for the post-transition corrosion of Zircaloy as a function of both time and temperature:

$$\Delta W = (B \exp[-Q_L/RT]\, t) + C. \quad (4)$$

Many early isothermal autoclave corrosion studies of the Zircaloys have been conducted, primarily in the temperature range of ~290–400°C [2–10]. In 1976 Hillner [11] compiled the data from Refs. [2–10] into engineering curves for each exposure temperature and, generating an activation energy for the post-transition rate constant, K_L, produced the following empirical expression for post-transition behavior:

$$\Delta W = 1.12 \times 10^8 \exp[-12\,529/T]\, t, \quad (5)$$

[1] 14.9 mg/dm^2 of weight gain = 1 μm of oxide growth = 0.66 μm of metal consumed.

where all of the terms have been defined previously. During the analyses of the Zircaloy corrosion data, the constant C was found to be small and not included in Eq. (5). (Note that for ease of calculation the parameter Q_L/R has been combined into a single value in the above equation.)

Several additional Zircaloy corrosion models have since been published in the technical literature [12–19]. Most modes follow the form of Eq. (4) for post-transition behavior and those that do not can be converted easily to this format. Comparisons with Eq. (5) have been conducted in many investigations [15–18,20–30]. Almost all of the early models suffer from one major weakness: there is a paucity of data for extended exposures in the post-transition region, especially at low temperatures. The Bettis Atomic Power Laboratory has generated a considerable quantity of autoclave corrosion data since the publication of Ref. [11]. The sections below present these new data and discuss the generation of new post-transition corrosion equations for the long-term autoclave exposure of Zircaloy.

3. New corrosion database

3.1. Test description for autoclave tests

Table 1 provides a summary of the material, test conditions, and the number of specimens employed in these experiments. All samples were either Zircaloy-2 or Zircaloy-4 compositions meeting the ASTM B-353 requirements. There were 278 specimens from 46 heats of material. Both thermal and anodic prefilms were included.

The tests were conducted in static isothermal autoclaves containing pH 7 water of five different temperatures; 270°C, 288°C, 316°C, 338°C and 360°C. There were single tests conducted at 270°C and 338°C, three tests at 288°C, seven at 316°C and ten at 360°C, for a total of 22 separate experiments. Specimen dimensions were typically 25 mm × 25 mm by ~1.5–2.5 mm thick. Sample preparation consisted of a pickle in 39 vol.% HNO_3 plus 3.5 vol.% HF, with H_2O as the remainder. A minimum of 50 μm of metal per surface was removed during pickling. The specimens were then rinsed in deionized water, dried, and weighed on a five-place balance prior to loading into the autoclaves. Periodic weight measurement were then obtained during exposure in the 22 different autoclave tests. At the completion of each periodic weight gain determination, the specimens were returned to their original autoclaves.

The number of specimens in each test decreased with increasing exposure since coupons were removed periodically for destructive analyses. For possible repository disposal application, long-term exposure data are of the most interest. Therefore, this analysis concentrated only on the post-transition kinetic region. It was assumed that weight gains of approximately 40–45 mg/dm^2 and above were in post-transition and the weight changes were tabulated from this point on. Maximum exposure time for any specimen was 10 507 days in a 316°C test (test #5) and the maximum weight gain was 1665 mg/dm^2 (~114 μm of oxide) in a 338°C experiment (test #12). The total database is comprised of approximately 14 500 data.

Table 1
Summary of material and test conditions

Test no.	Spec. no.[a]	Temp. (°C)	Material[b]	Heat treat[c]
1	4/4	270	Zr-2	α
2	10/9	288	Zr-2	α
3	6/5	288	Zr-2	α
4	6/5	288	Zr-4	α
5	5/5	316	Zr-2	α
6	5/5	316	Zr-2	α
7	3/3	316	Zr-2	α
8	15/3	316	Zr-2	α
9	20/9	316	Zr-4	α
10	15/3	316	Zr-4	α
11	21/9	316	Zr-4	α
12	6/3	338	Zr-2	α
13	7/6	360	Zr-4	α
14	2/2	360	Zr-4	α
15	7/7	360	Zr-4	α
16	4/4	360	Zr-4	β
17	3/3	360	Zr-2	α
18	17/6	360	Zr-2	α
19	71/57	360	Zr-4	α
20	12/12	360	Zr-4	α
21	29/27	360	Zr-4	α
22	10/9	360	Zr-4	α & β

[a] The number to the left of the / shows the number of specimens at the start of the post-transition period and the number to the right of the / shows the number of specimens at the completion of the test.
[b] Zr-2 denotes Zircaloy-2 samples. Zr-4 denotes Zircaloy-4 samples.
[c] α denotes final heat treatments in the alpha phase with typical equiaxed structures. β denotes a heat treatment in the beta phase with insufficient subsequent processing in the alpha phase to remove the lamella structure. Test 22 has samples of both types.

3.2. Test data

Specimen weight gains (mg/dm^2) were obtained for each specimen at each exposure time. The data were grouped by coupons that were nominally identical and tested together in the same autoclave in each test. The results were plotted on a single graph as a function of total exposure time (days). Each test was considered as a separate entity to prevent domination of the analysis by tests with many samples and weight-gain measurements.

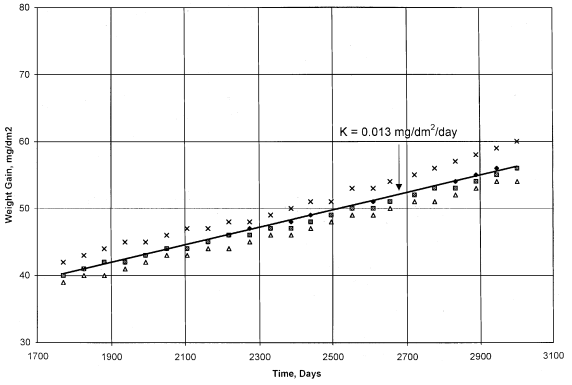

Fig. 2. Weight gain as a function of exposure time at 270°C, test no. 1.

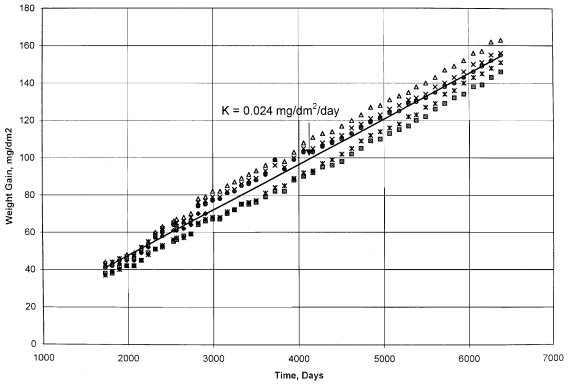

Fig. 3. Weight gain as a function of exposure time at 288°C, test no. 3.

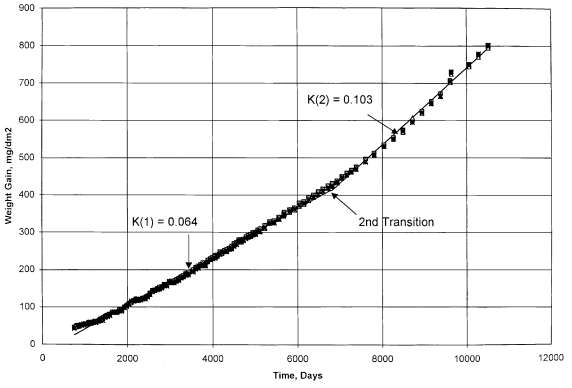

Fig. 4. Weight gain as a function of exposure time at 316°C, test no. 5.

The data at each temperature were plotted as a function of time, as illustrated in Figs. 2–6, and analyzed with a standard linear regression as per Eq. (2). All of the data

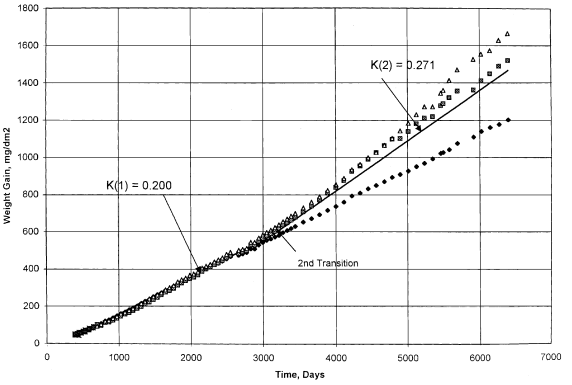

Fig. 5. Weight gain as a function of exposure time at 338°C, test no. 12. Note the difference in long-term post-transition corrosion behavior of one of the three specimens in this test.

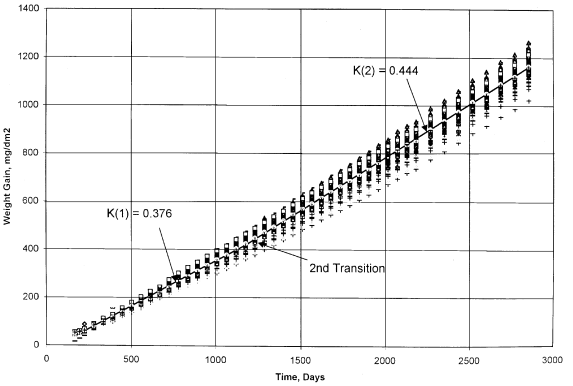

Fig. 6. Weight gain as a function of exposure time at 360°C, test no. 19.

generated in these tests are presented in Table 2. The data are divided into two separate groups: the data generated in the 270°C and 288°C tests and those from the higher temperature experiments. Thus, the data developed for each group of test temperatures are discussed separately.

3.2.1. 270°C and 288°C tests

As indicated above, only one experiment was conducted at 270°C and three tests were performed at 288°C. The weight gains generated as a function of exposure time for the four specimens in the 270°C test are shown in Fig. 2 along with the linear regression line fitted through the data. The linear rate constant $[K(1)]$ determined from these data (0.013 mg/dm^2/day) agrees favorably with that calculated from Eq. (5) (0.011 mg/dm^2/day). Although the total exposure time at this temperature (3000 days) is significantly longer than that of previous data, the maximum weight gain achieved

Table 2
Summary of linear and dual linear post-transition analyses

Test no.	Temp. (°C)	$K(1)$	$K(2)$	$C(2)$	Time tran.[a]	W tran.[b]	Time max[a]	W max[b]
1	270	0.013					3000	60
2	288	0.022					9347	229
3	288	0.024					6381	163
4	288	0.031					6381	203
5	316	0.064	0.103	−22.7	6874	419	10 507	801
6	316	0.077	0.110	−23.9	6461	473	10 059	912
7	316	0.085	0.107	−28.3	5855	472	8441	839
8	316	0.092	0.200	−26.5	4251	366	7039	943
9	316	0.075	0.122	−13.6	4320	310	7039	674
10	316	0.080	0.103	−17.9	4522	342	7039	600
11	316	0.078	0.135	−15.4	4498	334	7039	725
12	338	0.200	0.271	−41.8	3134	584	6392	1665
13	360	0.364	0.487	−22.4	679	225	1568	688
14	360	0.356	0.488	−18.8	720	237	1554	651
15	360	0.362	0.496	−18.2	672	225	1560	722
16	360	0.329	0.441	−7.7	493	154	1568	663
17	360	0.438	0.715	−38.0	887	351	1568	941
18	360	0.255	0.395	−7.8	869	214	1848	647
19	360	0.376	0.444	−24.2	1184	421	2854	1265
20	360	0.354	0.412	−20.4	1292	438	2854	1169
21	360	0.339	0.440	−18.4	1256	407	2854	1246
22	360	0.407	0.556	−4.1	1009	406	2730	1485

Transition time and transition weight gain are between stage 1 and stage 2 linear kinetics, i.e., 2nd transition.
[a] Time, in days.
[b] Weight gain, in mg/dm^2.

(60 mg/dm^2) is still considered to be at the very early stage of the post-transition kinetic region.

Fig. 3 shows the data for one of the three tests conducted at 288°C. As with the other two tests at this temperature, there is good fit between the data and the linear regression line. The three linear rate constants generated in these experiments were found to be 0.031, 0.024 and 0.022 mg/dm^2/day, in good agreement with the 0.023 mg/dm^2/day produced by Eq. (5).

3.2.2. 316°C, 338°C and 360°C tests

Unlike the lower temperature tests, the data generated at these elevated temperatures were found not to be in agreement with a single linear regression line for the entire post-transition period. Thus, the post-transition kinetic region can no longer best be described by a single post-transition rate constant, like that shown in Eqs. (2) and (3). The SOLO statistical software package was used to analyze the raw data and to generate algorithms that produced the best fit with the weight gain versus time data. A series of two successive linear equations, each active over a different time range, best describe the data. Figs. 4–6 show typical plots for the three elevated temperature test results. The solid lines in each plot show the result of the regression analysis for each set of data. The early linear portion of the post-transition region is designated as stage 1 and the later linear behavior stage 2. The software package automatically calculates both the time and weight gain at the transition point between the two linear stages. This latter transition point has been designated as the '2nd transition' to differentiate it from the earlier cubic-to-linear transition. Table 2 is a summary of all of the data generated in these experiments for both the single linear and dual linear post-transition kinetics.

3.3. Data analyses for temperature sensitivity

From the data in Table 2, the change from stage 1 to stage 2 linear kinetics occurs at about ~400 mg/dm^2. Since the weight gains developed in the two lower temperature tests have yet to achieve these values, there is no stage 2 linear kinetic region for these exposures.

As in the earlier studies, both stage 1 and stage 2 linear rate constants appear to follow an Arrhenius-type temperature dependence. Fig. 7 shows the natural logarithm of both linear rate constants plotted as a function of the inverse of the absolute temperature. Using standard linear regression, the following parameters were derived from Fig. 7 for the stage 1 post-transition region: $Q/R = 12\,880$ K with the pre-exponential constant $(B) = 2.47 \times 10^8$ mg/dm^2/day. The corresponding values

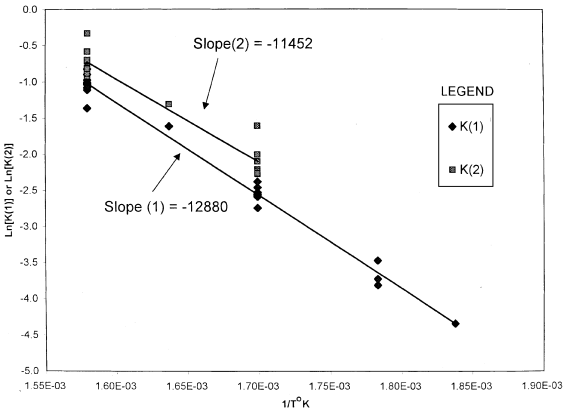

Fig. 7. The natural logarithm of the stage 1 and stage 2 linear rate constants as a function of the inverse absolute temperature (K).

for the stage 2 kinetic region are 11 452 K and 3.47×10^7 mg/dm^2/day, respectively. Thus, the stage 1 linear rate constant as a function of temperature $[dW(1)/dt]$ is given by

$$dW(1)/dt = K(1) = 2.47 \times 10^8 \exp[-12\,880/T] \text{ mg/dm}^2\text{/day}, \quad (6)$$

and the corresponding rate constant for the second-stage linear corrosion is

$$dW(2)/dt = K(2) = 3.47 \times 10^7 \exp[-11\,452/T] \text{ mg/dm}^2\text{/day}. \quad (7)$$

Since $K(2)$ is always equal to or slightly greater than $K(1)$, and it is assumed that the Zircaloy cladding on the expended fuel elements will be in the post-transition kinetic region upon disposal, the use of Eq. (7) to estimate the amount of additional corrosion due to repository exposure is conservative. Eqs. (6) and (7) are known to be valid within the database used for their generation, which is up to approximately 114 μm of oxide film. Extrapolations beyond 114 μm film thicknesses may include a risk of another transition to a region with faster corrosion.

3.4. In-reactor tests

Before the first transition from cubic to linear kinetics, corrosion rates are the same in and out of reactor. After this transition, corrosion is more rapid in reactor than out of reactor. As discussed below, two investigations indicate that this acceleration in corrosion rate disappears after the oxide formed in reactor is separated from the base metal by about 30 mg/dm^2 of oxide formed out of reactor. To verify this decaying memory effect, special in-reactor corrosion tests were performed in the Advanced Test Reactor. Zircaloy-4 corrosion coupons were initially exposed in one set of conditions and then exposed to a different set of conditions. Control coupons were exposed to the same conditions throughout. Weight gains were periodically performed.

Fig. 8(a) shows the corrosion of a Zircaloy-4 coupon exposed in ATR at about 270°C for 2500 days, initially at high flux with several decreases in flux to one-third of the initial flux, as shown in the irradiation history provided in Fig. 8(b). Fig. 8(a) also shows the corrosion of coupons exposed to the irradiation history of Fig. 8(c), a nearly constant high-flux level that is comparable to the average level of Fig. 8(b). As the data for the coupon corresponding to the history of Fig. 8(b) show, the irradiation flux level has no effect on the corrosion rate during the pre-transition period of approximately the first 1000 days. However after this pre-transition period, the corrosion rate increases beyond what would be expected for the irradiation flux level during this time, based on isoflux tests. In fact, the rate is higher at this time than the nearly constant high-flux data of samples irradiated with the history of Fig. 8(c). Finally, after another 500 days, the corrosion rate has decreased to a rate that is now less than the rate of the samples of Fig. 8(c), even though those samples have experienced about the same average irradiation flux level. The important memory-related results of this test are that: (1) the initial high-flux period during the first 500 days was not reflected in the corrosion rate until about 1200 days, when the sample left the pre-transition period, and (2) the decrease in flux to below that of the flux of the other samples, just as the sample left the pre-transition period at about 1200 days, was not reflected in the corrosion rate until about 500 days later at 1700 days, after which the corrosion rate became less than that of the other samples. This demonstrates that decreases in neutron irradiation flux are not initially reflected in corrosion rate; but after additional corrosion of 1–2 μm, corrosion rates decrease.

This memory effect also is illustrated in a coupon initially irradiated for about 100 days at a high temperature 360°C and then irradiated at a low temperature 270°C. The control samples are the same ones as for the above illustration, being irradiated at low temperature throughout their exposure. The result is shown in Fig. 9(a). During the ~100 days at 360°C approximately 10 μm (0.4 mils) of corrosion occurred. Immediately upon lowering temperature to 270°C and increasing flux, as shown in Fig. 9(b), the corrosion rate decreases to a lower rate than expected for the existing corrosion thickness, as shown in Fig. 9(a), which also shows the corrosion rate for coupons exposed isothermally at 270°C. Approximately 1000 days at 270°C are required before the corrosion rate of the temperature-shifted

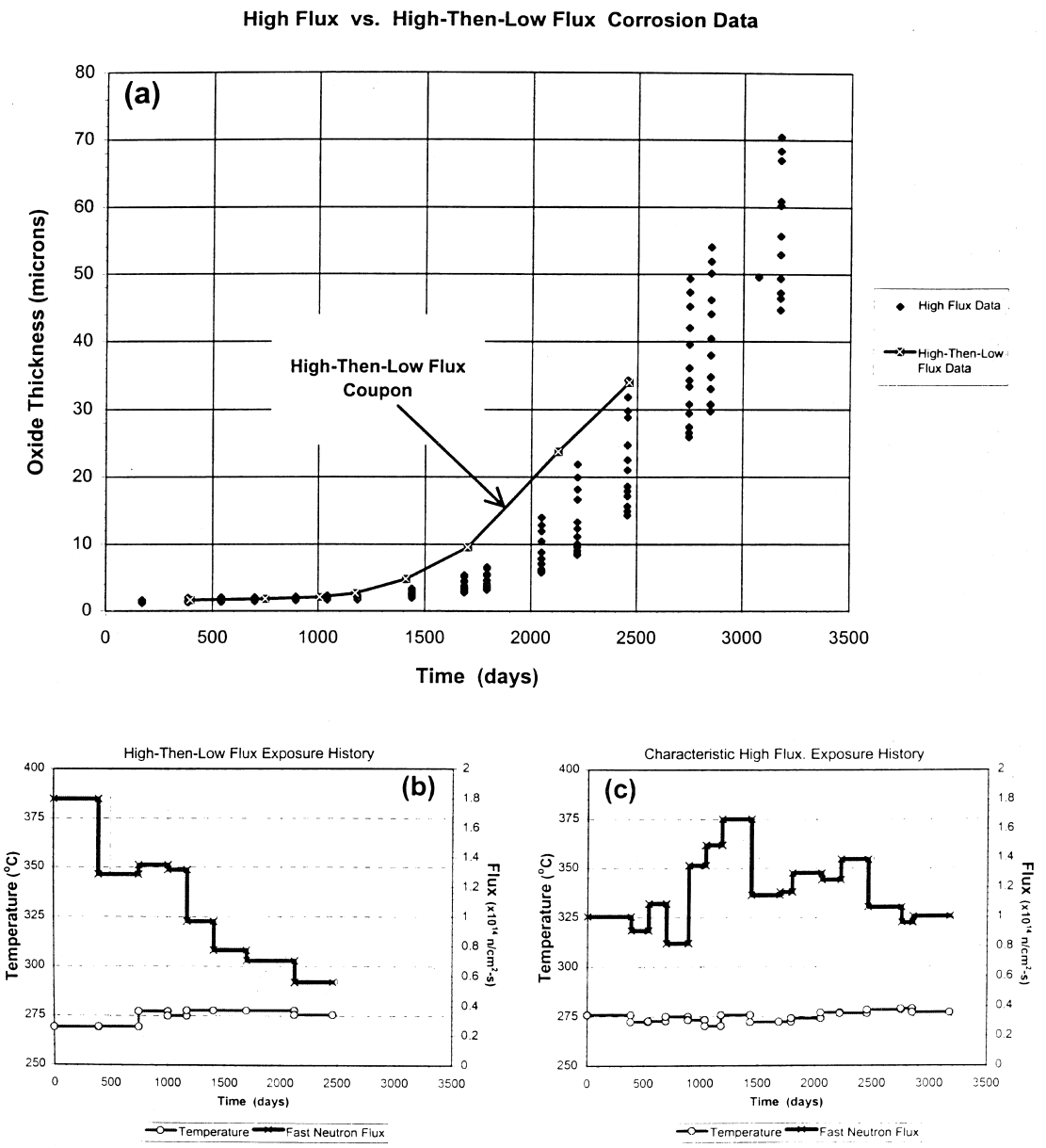

Fig. 8. Effect of shift in neutron flux on subsequent in-pile corrosion rate.

sample becomes similar to that of isothermally exposed samples. During exposure at 360°C much of the irradiation effect on the Zircaloy-4 is annealed relatively quickly. As a result, the corrosion rate immediately following the temperature change to 270°C initially is more representative of non-irradiated material than material irradiated at 270°C. After about 1000 days at 270°C, irradiation damage produces a material representative of material irradiated isothermally at 270°C and the corrosion rate also becomes the same. A similar memory effect, out-of-pile, has been reported by Beie et al. [31].

4. Discussion

For the possible application of the new database to repository disposal conditions, it is of interest to compare predictions from various corrosion models for prolonged exposure to a low-temperature environment. Rothman [20] considered a constant temperature of 180°C for 10 000 yr. Using Rothman's exposure conditions, calculations were conducted with nine different corrosion correlations reported in the literature and the results reported here as Eqs. (6) and (7). Table 3 shows

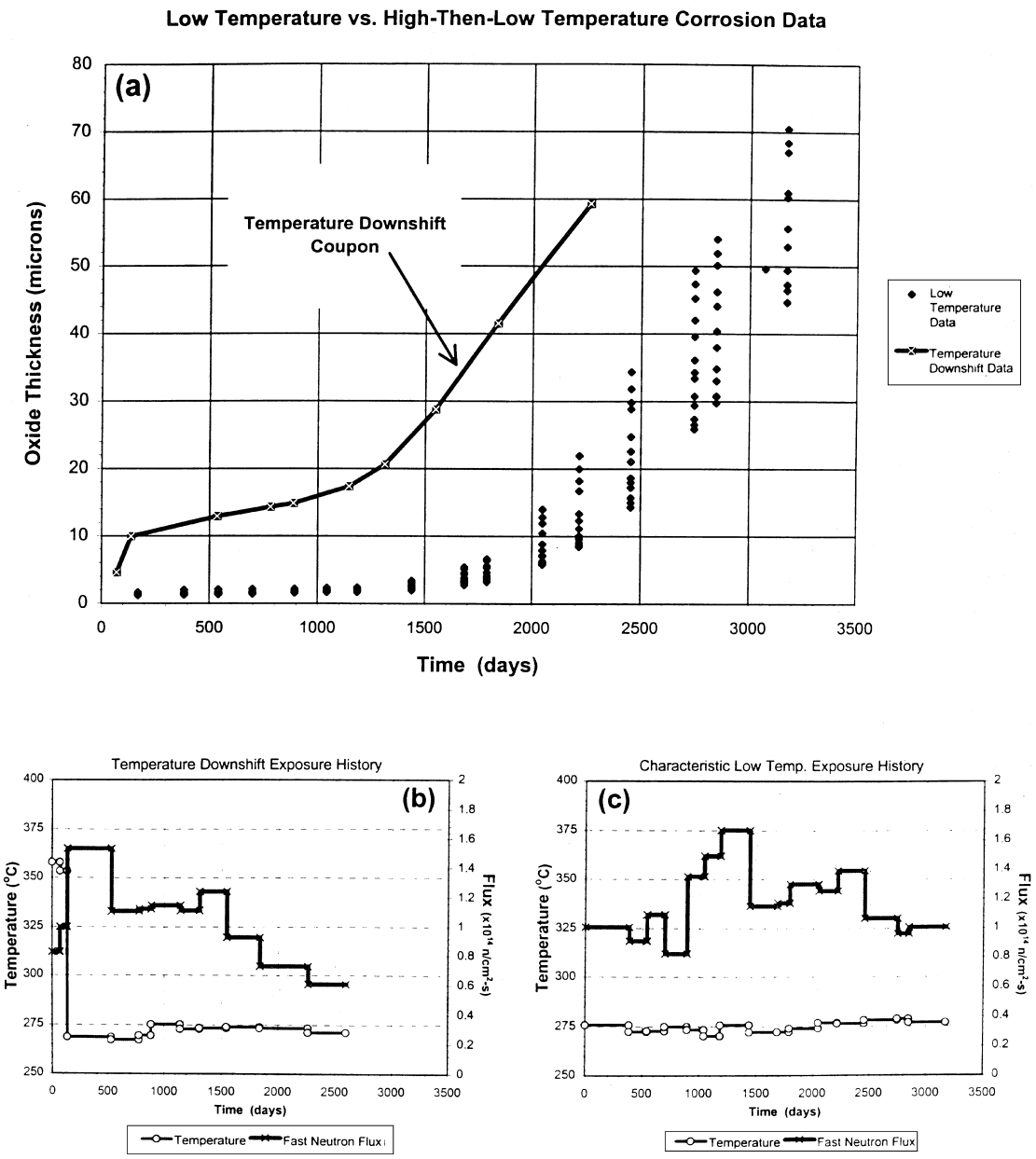

Fig. 9. Effect of shifts in temperature and neutron flux on subsequent in-pile corrosion rate.

the results of such calculations. The prediction for Ref. [11] model was based on the use of Eq. (5). All of the numbers in Table 3 have been rounded.

For 10 000 yr at 180°C, Eq. (6) predicts an additional oxide film growth of ~27 μm (which is identical to that predicted by Eq. (5), whereas Eq. (7) produces an oxide film thickness growth of ~89 μm. There is good agreement between the new stage 1 post-transition linear rate equation (Eq. (6)) and the earlier-reported post-transition kinetics in Eq. (5). In this region of agreement the oxide thicknesses are similar. The stage 2 oxide rates, Eq. (7), and the amounts of oxide predicted, are significantly greater than those estimated from the literature correlations. This is due to the literature correlations being based on relatively thin oxides.

There have been several additional algorithms reported in the literature for the oxidation of Zircaloy at elevated temperatures. For example, Boase and Vandergraaf [32] show an Arrhenius-type plot of rate constants compiled from various documents (some

Table 3
Comparison of predictions from 10 models for the corrosion of Zircaloy after 10 000 yr at 180°C

Investigator [Ref.]	B	Q_L/R	K_L	ΔW (mg/dm^2)	Thickness (μm)
Hillner [11]	1.12×10^{8}	12 529	1.10×10^{-4}	402	27
van der Linde [12]	2.30×10^{9}	14 451	3.25×10^{-5}	119	8.0
Dyce [13]	6.53×10^{9}	15 109	2.16×10^{-5}	79	5.3
Dalgaard [14]	1.84×10^{7}	11 222	3.23×10^{-4}	1181	79
Billot [15]	1.13×10^{8}	12 567	4.95×10^{-5}	181	12
Garzarolli [16]	1.18×10^{9}	13 815	1.02×10^{-4}	374	25
Stehle [17]	2.21×10^{9}	14 242	6.80×10^{-5}	248	17
Peters [18]	8.12×10^{8}	13 512	9.12×10^{-5}	333	22
MATPRO [19]	1.23×10^{9}	14 080	3.94×10^{-5}	143	9.6
This work, Eq. (6)	2.47×10^{8}	12 880	1.12×10^{-4}	409	27
This work, Eq. (7)	3.47×10^{7}	11 452	3.67×10^{-4}	1341	89

unpublished) with wet and dry air and steam in the temperature range range ~298–725°C. Similarly, Suzuki and Kawasaki [33] report on the oxidation of Zircaloy in moist air in the temperature range 350–500°C. Einziger [34] generated an equation for Zircaloy oxidation based upon the work of the previous two references. The results of these studies were not included in the comparisons of Table 3 because of differences in test conditions, i.e., temperature or environment. Inclusion of these reported corrosion rates would not have altered the results of this study, despite the differences in test conditions. For all conditions discussed to date, including the information presented above in Refs. [32–34], Eq. (7) of this report produces the most-conservative estimate of additional oxide buildup on spent Zircaloy-clad fuel assemblies due to long-term exposure to expected geologic repository conditions. These maximum corrosion rates are due to the underlying database that includes the thickest corrosion films reported to date (up to 114 μm) at relatively low temperatures.

4.1. Effect of prior irradiation

The predictions for the additional corrosion on the Zircaloy cladding during repository disposal presented above were based on isothermal autoclave testing of non-irradiated specimens. However, it has been shown that when Zircaloy is transferred from an aggressive environment to one that is considerably less aggressive, the corrosion rate may continue at the more aggressive rate for some period of time. This behavior has been termed the 'memory' effect. Thus, the corrosion of cladding that has experienced appreciable irradiation exposure prior to disposal in a repository may be accelerated, especially for the post-transition kinetic regime. At the present time it is uncertain how long this accelerated in-reactor corrosion rate will persist when transferred to an ex-reactor corrosion environment, but sufficient data are available to bound the effect.

Garzarolli et al. [16] conducted an experiment to determine how rapidly the enhanced corrosion rate observed in-reactor would decrease to that anticipated from ex-reactor (autoclave) date. The authors found that samples of cladding from a BWR that were irradiated at an estimated temperature of 290°C continued to corrode at the irradiated rate for the first ten days in an autoclave at 280°C. In the time frame from 10 to 110 days the rate continued to decrease until, at 110 days, it became close to that measured in autoclave testing of non-irradiated specimens. When exposed to higher temperatures in autoclaves (300–350°C) the specimens were found to attain the ex-reactor rate quickly. At the highest autoclave temperature there appeared to be no memory effect of the prior irradiation exposure, i.e., the measured corrosion rate agreed very favorably with the ex-reactor rate from the onset of the high-temperature post-transition autoclave exposure.

Somewhat different results were obtained with specimens from cladding taken from PWRs (Figs. 4-13–4-16 in Ref. [16]). In one batch of irradiated specimens tested in autoclaves at temperatures up to 350°C, the corrosion rate measured after the first cycle of exposure in the autoclave at 280°C was a factor of 20 greater than the non-irradiated corrosion rate. However, this accelerated rate decreased to a factor of 2 or less during subsequent autoclave exposures when temperature was increased and time was about 140 days. The test was terminated after 260 days in the autoclave. It is not known whether additional long-term autoclave exposure would have resulted in the convergence of the post-irradiated and non-irradiated corrosion rates, since neither the PWR nor the BWR specimens being tested at 280°C continued until convergence was achieved. At a higher autoclave temperature (350°C) the corrosion rate for the PWR specimens agreed very well with the expected non-irradiated corrosion rate after considerable times at lower temperatures. In all cases, the effect of irradiation was reduced to a factor of 2 or less on or before 110 days of post-irradiation exposure at 280°C.

Cheng et al. [35] also investigated post-irradiation corrosion performance of Zircaloys. However, these authors removed the in-reactor oxide film and pickled the surface on almost all of their samples before post-irradiation autoclave exposure. The oxide was removed because they were concentrating on determining the effect of irradiation on corrosion rates through irradiation-induced dissolution of second-phase particles in the metal. With the exception of two of the weld metal samples, all samples post-irradiation tested at 316°C corroded at essentially the same rate as non-irradiated samples, despite the irradiation-induced changes in microstructure and dissolution of alloying elements into the zirconium matrix, which Cheng et al. confirmed. Two of the weld metal samples post-irradiation tested at 316°C corroded at higher rates than the other samples. This was attributed to the strong susceptibility of weld-metal precipitates to an irradiation-induced dissolution. There was no explanation as to why some weld metal samples corroded at an accelerated rate and some at the corrosion rate of non-irradiated material. However, all base metal samples corroded at the non-irradiated rate, not showing the memory effect reported by Garzarolli. This would suggest that the memory effect at 316°C is associated with the effect of irradiation on the oxide films rather than on the base metal. This interpretation is somewhat different from that given by Cheng et al. The modified interpretation is necessary to reconcile the post-transition corrosion observations of both Garzarolli and Cheng for post-irradiation testing with and without the in-reactor oxide removed.

Cheng also post-irradiation tested the samples at 400°C and observed accelerated corrosion. For samples with the oxide removed, the corrosion rate was initially high but decreased with post-irradiation exposure. This decrease in rate was associated with precipitation of alloying elements during post-irradiation testing, which occurred at 400°C but not at 316°C. One sample post-irradiation tested at 400°C with the in-reactor corrosion film left on behaved differently from the samples post-irradiation tested at 400°C with the in-reactor corrosion films removed. The sample with the in-reactor corrosion film left on initially corroded at a slow rate that was more like the in-reactor rate than the 400°C rate, suggesting that the character of the oxide initially controlled the rate in this case. After some time, the corrosion rate for the sample with the in-reactor oxide left on increased to a similar rate as the post-irradiation rate of the samples with the in-reactor oxides removed.

The testing of Garzarolli et al. and Cheng et al. suggest that there are two post-irradiation time-dependent effects of in-reactor irradiation on post-irradiation corrosion rates. The first effect is on the oxide. This effect is a post-irradiation corrosion-rate acceleration that decays relatively rapidly, at least rapidly compared to repository times, to less than a factor of 2 of the non-irradiated post-transition corrosion rate at 316°C and lower. The second effect is on the metal. At relatively high temperatures the alloying elements that became supersaturated by the irradiation-induced dissolution begin to precipitate in a unique microstructure that increases the corrosion rate at 400°C. This unique microstructure and the associated acceleration in corrosion rate may not occur at 316°C. Other investigators have observed the temperature dependence on post-irradiation microstructural changes at high temperatures. For usual repository conditions the temperatures are never high enough to induce such microstructural changes. Therefore, the testing at 316°C and below by both Garzarolli et al. and by Cheng et al., despite Cheng's removal of the oxide, support the assumption that the post-irradiation repository corrosion rates will be within a factor of two of the non-irradiated post-transition corrosion rates reported and modeled above.

These post-irradiation corrosion test results suggest that it is possible for PWR Zircaloy cladding in a repository to experience an enhanced corrosion rate over that predicted from autoclave test data. An conservative treatment is to assume that the corrosion rate at the low repository temperatures will never converge to the pre-irradiation rate. Applying a factor of 2 to the corrosion rate can reflect this uncertainty.

5. Conclusions

Only single linear post-transition rate constants were found for the 270°C and 288°C tests instead of the dual linear rate constants observed in the higher temperature experiments. Undoubtedly, the corrosion thicknesses at these low temperatures were too thin to have reached the 2nd transition and stage 2 kinetic region. The rate constant determined for the stage 1 post-transition kinetic region (Eq. (6)) agrees favorably with the much-earlier-developed rate constant for the early post-transition period (Eq. (5)). However, extrapolation of Eq. (5) to higher temperatures and longer exposure times would never have predicted the 2nd transition and onset of stage 2 kinetics. This exercise underscores the caution that must be associated with extrapolations beyond the limits of the database. Thus, it has been shown that specimens with oxide film thicknesses in excess of $\sim$30 μm will corrode at an increased linear post-transition rate compared to specimens in the post-transition kinetic region with oxide films thinner than this value. The reason for this increased corrosion rate for the thicker films is not readily apparent.

Within a single autoclave experiment, sample-to-sample long-term post-transition kinetics varied from little effect to appreciable differences. Maximum deviations were seen in the single test at 316°C (Fig. 4), where one of the three specimens that had experienced the

maximum exposure time exhibited no 2nd transition or stage 2 kinetics, even after attaining a weight gain of 1200 mg/dm^2 ($\sim$80 μm). Fig. 6 shows the data developed in a 360°C test where a total of 57 specimens were exposed for the entire post-transition period; considering the number of specimens involved, the sample-to-sample deviations appear minimal.

Prior exposure to irradiation will accelerate corrosion until several microns of additional oxide thickness form. Afterwards, the corrosion rates return to that of Zircaloy with no prior irradiation. For long-term exposures, the effect of prior irradiation can be treated either by adding 3 μm of oxide to that estimated from Eq. (7) or by applying a factor of 2 to Eq. (7). The latter is more conservative.

Application of the new corrosion correlations developed in this report to repository disposal conditions may require the application of a factor of 2 increase in the corrosion rate to reflect the uncertainty associated with the post-irradiation corrosion behavior of irradiated cladding.

Acknowledgements

The authors wish to acknowledge the direction supplied by, and the many helpful discussions held with, Mr Bruce F. Kammenzind and the assistance of Ms Cheryl Hall in all phases of data collection, collation and transmittal is also acknowledged. The authors also wish to express their appreciation to Mr Walter Meyers for all calculations conducted with the SOLO computer program and for the statistical review of this paper.

References

[1] J.S. Bryner, J. Nucl. Mater. 82 (1979) 84.
[2] D.E. Thomas, in: B. Lustman, F. Kerze (Eds.), Metallurgy of Zirconium, McGraw-Hill, New York, 1955, p. 608.
[3] S. Kass, in: Proceedings of US Atomic Energy Commission Symposium on Zirconium Alloy Development, Castlewood, Pleasanton, CA, USA, 12–14 Nov. 1962, p. 1-1.
[4] S. Kass, in: Corrosion of Zirconium Alloys, ASTM STP 368, American Society for Testing and Materials, Philadelphia, 1964, p. 3.
[5] D.E. Thomas, in: Proceedings of International Conference on the Peaceful Uses of Atom Energy, vol. 9, United Nations, Geneva, 1955, p. 407.
[6] J.N. Chirigos et al., in: Proceedings of Fuel Element Fabrication with Special Emphasis on Cladding Materials, vol. 1, Academic Press, New York, 1961, p. 19.
[7] S. Kass, Corrosion 23 (1967) 374.
[8] J.E. Draley et al., in: Proceedings of Third International Conference on the Peaceful Uses of Atomic Energy, vol. 9, United Nations, Geneva, 1964, p. 470.
[9] S. Kass, W.W. Kirk, Trans. Am. Soc. Met. 55 (1962) 77.
[10] S. Kass, The corrosion and hydrogen pickup of electron beam welded nickel-free Zircaloy-2 and Zircaloy-4, Westinghouse Electric Corporation Report WAPD-TM-533, March 1966.
[11] E. Hillner, in: A.L. Lowe Jr., G.W. Parry (Eds.), Zirconium in the Nuclear Industry, ASTM STP 633, American Society for Testing and Materials, Philadelphia, 1977, p. 211.
[12] A. van der Linde, Calculation of the safe lifetime expectancy of zirconium alloy canning in the fuel elements of the NERO reactor, Reactor Centrum Nederland Report RCN Report 41, July 1965.
[13] I.H. Dyce, Nucl. Eng. 9 (98) (1964) 253.
[14] S.B. Dalgaard, in: Extended Abstracts of the Electrochemical Society, Washington, DC, USA, 2–7 May 1976, 76-1, p. 82.
[15] P. Billot, P. Beslu, A. Giordano, J. Thomazet, in: L.F.P. Van Swam, C.M. Eucken (Eds.), Eighth International Symposium on Zirconium in the Nuclear Industry, ASTM STP 1023, American Society for Testing and Materials, Philadelphia, 1989, p. 165.
[16] F. Garzarolli, W. Jung, H. Schoenfeld, A.M. Garde, G.W. Parry, P.G. Smerd, Waterside corrosion of Zircaloy fuel rods, EPRI NP-2789, December 1982.
[17] H. Stehle, W. Kaden, R. Manzel, Nucl. Eng. Des. 33 (1975) 155.
[18] H.R. Peters, H.R., in: D.G. Franklin, R.B. Adamson (Eds.), Sixth International Symposium on Zirconium in the Nuclear Industry, ASTM STP 824, American Society for Testing and Materials, 1984, p. 507.
[19] MATPRO: Version 10, A Handbook of Materials Properties for Use in the Analysis of Light Water Reactor Fuel Rod Behavior Report TREE-NUREG-1180, 1978.
[20] A.J. Rothman, Potential corrosion and degradation mechanisms of Zircaloy cladding on spent nuclear fuel in a tuff repository, Lawrence Livermore National Laboratory Report UCID-20172, 1984.
[21] A.B. Johnson Jr., Behavior of spent nuclear fuel in water pool storage, Pacific Northwest Laboratories Report BNWL-2256, 1977.
[22] D.D. Lanning, A.B. Johnson Jr., D.J. Trimble, S.M. Boyd, in: L.F.P. Van Swam, C.M. Eucken (Eds.), Eighth International Symposium on Zirconium in the Nuclear Industry, ASTM SP 1023, American Society for Testing and Materials, Philadelphia, 1989, p. 3.
[23] R.A. Graham, J.P. Tosdale, P.T. Finden, in: L.F.P. Van Swan, C.M. Eucken (Eds.), Eighth International Symposium on Zirconium in the Nuclear Industry, ASTM STP 1023, American Society for Testing and Materials, Philadelphia, 1989, p. 334.
[24] F. Garzarolli, D. Jorde, R. Manzel, J.R. Politano, P.G. Smerd, in: D.G. Franklin (Ed.), Fifth Conference on Zirconium in the Nuclear Industry, ASTM STP 754, American Society for Testing and Materials, 1989, p. 430.
[25] A.B. Johnson Jr., Bases for extrapolating materials durability in fuel storage pools, Pacific Northwest Laboratory Report PNL-SA-24126, 1994.
[26] R.A. Graham, C.M. Eucken, Zirconium in the Nuclear Industry: Ninth International Symposium ASTM STP 1132, in: C.M. Eucken, A.M. Garde (Eds.), American

Society for Testing and Materials, Philadelphia, 1991, p. 279.
[27] T. Isobe, Y. Matsuo, in: C.M. Eucken, A.M. Garde (Eds.), Ninth International Symposium on Zirconium in the Nuclear Industry, ASTM STP 1132, American Society for Testing and Materials, Philadelphia, 1991, p. 346.
[28] V.F. Urbanic, R. Choubey, C.K. Chow, in: C.M. Eucken, A.M. Barde (Eds.), Ninth International Symposium on Zirconium in the Nuclear Industry, ASTM STP 1132, American Society for Testing and Materials, Philadelphia, 1991, p. 665.
[29] D. Pecheur, A. Lefebvre, T. Motta, C. Lemaignan, C. Charquet, in: A.M. Garde, E.R. Bradley (Eds.), Tenth International Symposium on Zirconium in the Nuclear Industry, ASTM STP 1245, American Society for Testing and Materials, Philadelphia, 1994, p. 687.
[30] A.M. Garde, S.R. Pati, M.A. Krammen, G.P. Smith, R.K. Endter, in: A.M. Garde, E.R. Bradley (Eds.), Tenth International Symposium on Zirconium in the Nuclear Industry, ASTM STP 1245, American Society for Testing and Materials, Philadelphia, 1991, p. 760.
[31] H.J. Beie, A. Mitwalsky, F. Garzarolli, H. Ruhmann, H.J. Sell, in: A.M. Garde, E.R. Bradley (Eds.), Tenth International Symposium on Zirconium in the Nuclear Industry, ASTM STP 1245, American Society for Testing and Materials, Philadelphia, PA, 1994, p. 61.
[32] D.G. Boase, T.T. Vandergraaf, Nucl. Technol. 32 (1977) 60.
[33] M. Suzuki, S. Kawasaki, J. Nucl. Mater. 140 (1986) 32.
[34] R.E. Einziger, in: Proceedings of Fifth Annual International Conference, Las Vegas, Nevada, 22–26 May 1994, vol. 2, American Nuclear Society, La Grange Park, IL, 1994, p. 554.
[35] B.C. Cheng, R.M. Kruger, R.B. Adamson, in: A.M. Garde, E.R. Bradleyh (Eds.), Tenth International Symposium on Zirconium in the Nuclear Industry, ASTM STP 1245, American Society for Testing and Materials, Philadelphia, 1994, p. 400.